Int. J. Multiphase Flow Vol. 8, No. 5, pp. 509–524, 1982
Printed in Great Britain.

0301-9322/82/040509-16$03.00/0
Pergamon/Elsevier

FLOW PATTERN TRANSITION FOR GAS-LIQUID FLOW IN A VERTICAL ROD BUNDLE

P. VENKATESWARARAO, R. SEMIAT* and A. E. DUKLER

University of Houston, Houston, TX 77004, U.S.A.

(*Received* 30 *August* 1981; *in revised form* 29 *December* 1981)

Abstract—Experimental and analytical studies are presented directed to the prediction of flow pattern transitions in a vertical rod bundle array. The test section used consists of a 24 rod matrix on a square pitch in a cylindrical shell. Analytical models are given based on physical interpretation of the transition mechanisms. Data on rise velocities of small and large bubbles in rod bundles are also presented.

INTRODUCTION

This study of flow pattern transitions in rod bundles was motivated by the need for predicting such transitions in a pressurized water nuclear reactor during a loss of coolant accident (LOCA). During such an accident two phase flow takes place in the space between the rods, and reliable calculation of the flow and heat transfer rates depends on being able to predict the flow pattern. Flow pattern transition information is also useful for analysis and design of two phase flow on the shell side of heat exchanger tube bundles.

Experiments involving the transitions in rod bundles are few in number and no theory has appeared in the literature. Bergles *et al.* (1968) studied the two phase upflow of steam-water at a pressure of 6.9×10^6 N/m^2 in a four rod bundle arranged in a square array. Similar studies were undertaken by Williams & Peterson (1978) at 2.76×10^6, 8.27×10^6 and 13.79×10^6 N/m^2 in a four rod bundle arranged in a linear array. In both studies bubble, froth, slug and annular flows were observed. Williams & Petersons data (1978) show that some of the flow patterns may be absent at certain pressures and flow rates.

To understand the flow pattern transition in a rod bundle, a test section with 24 rods, arranged on a square pitch in a cylindrical shell was constructed and the upflow of air–water was studied. This paper presents the results of these experiments and suggests a mechanistic basis for the prediction of flow pattern transition following the modelling ideas proposed by Taitel & Barnea (1980).

EXPERIMENTAL

The flow loop is shown schematically in figure 1. Figure 2 gives a dimensional sketch of the test section assembly. Water is supplied to the test section through the conical section shown at the bottom.

A variety of methods were used to generate bubbles for the measurement of rise velocity. For large Taylor bubbles an inverted Plexiglas hemisphere as shown above the water entry in figure 2 was loaded with air from a calibrated syringe or from the air supply tube and manually inverted to create the bubble. Small Taylor bubbles which occupied the space between four rods were generated by removing the cap and pulsing the air flow using a timed solenoid on the air supply tube. For continuous gas flow the gas entry section was replaced with one shown in cross section in figure 3 equipped with four 0.64 cm and four 1.27 cm diameter ports located around the perimeter of the shroud. This entry section was used for all flow pattern transition studies. Small bubbles were generated using the entry by inserting a plate having one centered orifice just below the rod bundle. Water and gas flowing up the rod bundle overflowed at the top into a plastic drum which served as a separator. The water was returned to the supply tank while air was exhausted into the atmosphere.

A cross sectional view of the rod bundle appears in figure 4. The rods were 1.27 cm in diameter and are arranged in a square pitch of 1.75 cm. The cylindrical shell had an i.d. of

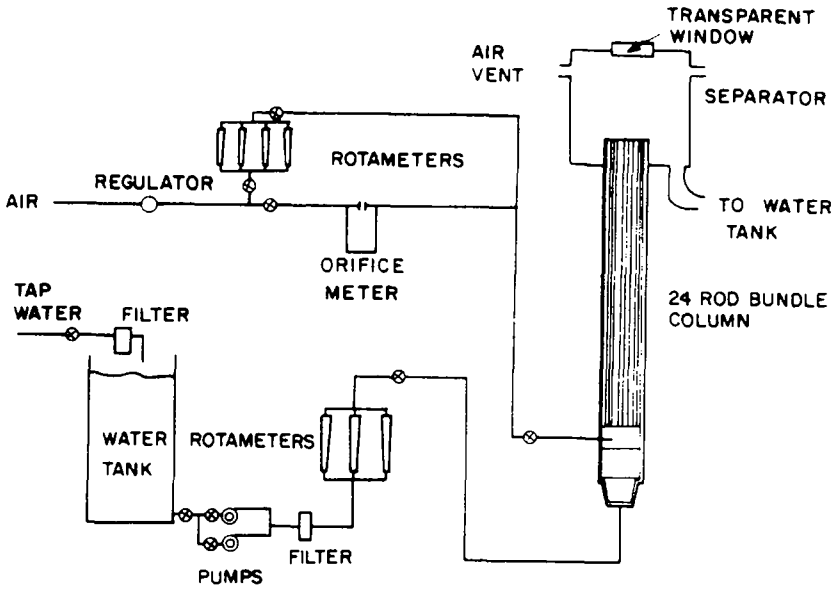

Figure 1. Flow loop.

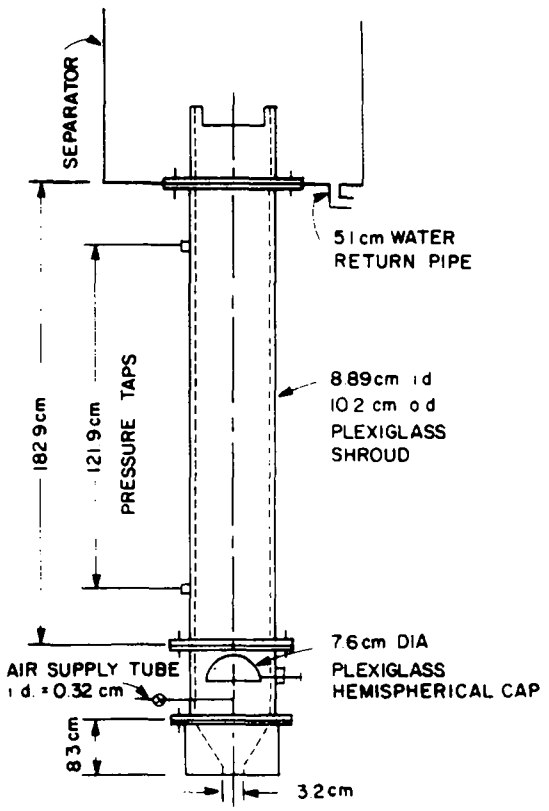

Figure 2. Test section assembly.

8.89 cm with 0.64 cm wall thickness. Both rods and shell were made of transparent Plexiglas to permit visual observation of the flow patterns. Partial rods at the wall were used to minimize bypassing and to create a true section of a larger bundle. Vibration of the rods was eliminated by using Plexiglas pins between rods at random locations. The entire rod system was assembled on steel cross rods located at the top and bottom. At the top these steel rods extended beyond the rod matrix and were used to support the rod bundle by resting these rods in a cut-out shown

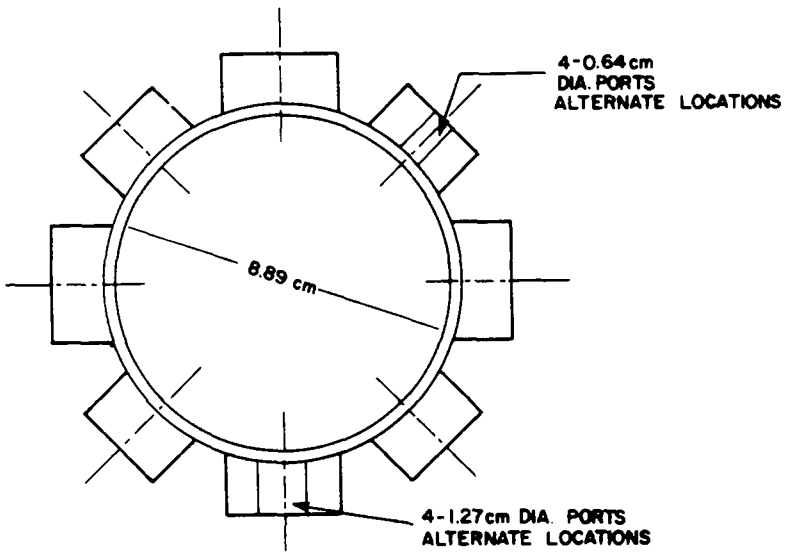

Figure 3. Entry section for continuous gas flow.

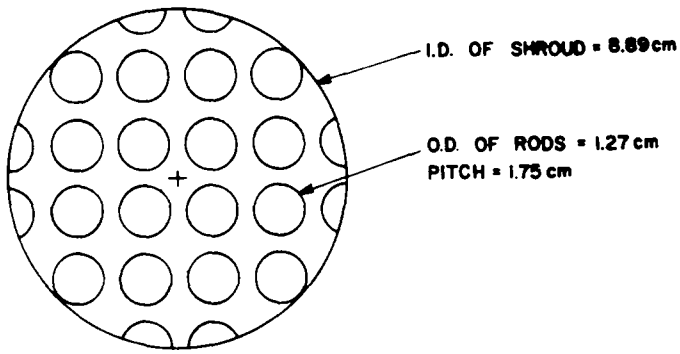

Figure 4. Cross section of rod bundle.

at the top of the assembly in figure 2. The partial rods shown in figure 4 were screwed to the cylindrical shroud to minimize bypassing along the wall. Pressure taps were installed 122 cm apart on the test section. Details of the equipment along with photographs are given by Venkateswararao (1981).

Velocities of large bubbles (10–80 cm^3) were measured using high speed photography and a timing clock in the background having a resolution of 0.01 second. Velocity and size of small bubbles were measured using the laser/Ronchi grating technique developed by Semiat & Dukler (1981). Flow patterns were observed visually.

EXPERIMENTAL RESULTS

Based on visual observations, the following flow patterns were observed over the range of flow rates possible with the air and water supply system.

Bubble flow. Bubbles whose diameters are less than the characteristic spacing between the rods, flow upward, distributed in the liquid phase.

Slug flow. Large bubbles move upward, followed by a liquid slug carrying small distributed bubbles. The liquid around the large bubble flows down as a film along the rods. Two types of large bubbles are observed as shown in figure 5: (a) Large Taylor type bubbles whose caps are penetrated by a number of rods. In some cases these bubbles are large enough to occupy almost the entire cross sectional area of the cylindrical shell. These are designated as *shroud Taylor bubbles.* In general, shroud Taylor bubbles are observed only when there is a sudden increase in

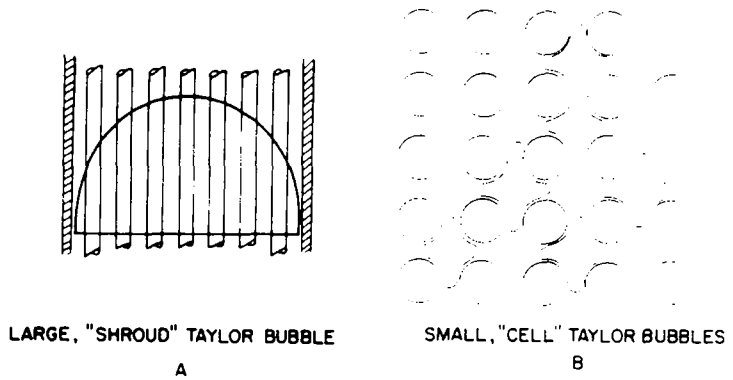

Figure 5. Two types of Taylor bubbles.

the gas flow rate. (b) Nearly sphericallly capped bubbles ocoupying the space in a four rod cell whose caps are not penetrated by the rods. Such bubbles are designated as *cell Taylor bubbles.*

Churn flow. This flow patttern is characterized by irregular alternating motion of liquid and gas. In slug flow the propagation velocities of the large bubbles and the liquid slugs are always uniformly upward while that of the film alongside the bubble is uniformly downward. During churn flow the direction of the liquid flow changes in an erratic and irregular way from upflow to downflow and vice versa. Liquid flows downward not only as a film but also as units of liquid which occupy much of the cross sectional area, are collected at lower positions and forced to rise again by liquid and gas from below.

Annular flow. Liquid flows as a wavy film along the rods and the shroud while part of the liquid is carried by the gas as dispersed droplets.

Flow patterns as observed over the operable flow rate range are shown in figure 6. The solid curves indicate the location of the experimentally observed variations. Measured pressure gradients appear in figure 7.

BUBBLE RISE VELOCITIES

Small bubbles. Bubble size and rise velocities were measured for (a) separated non-interacting bubbles in the absence of liquid feed, (b) separated bubbles in a moving liquid (30

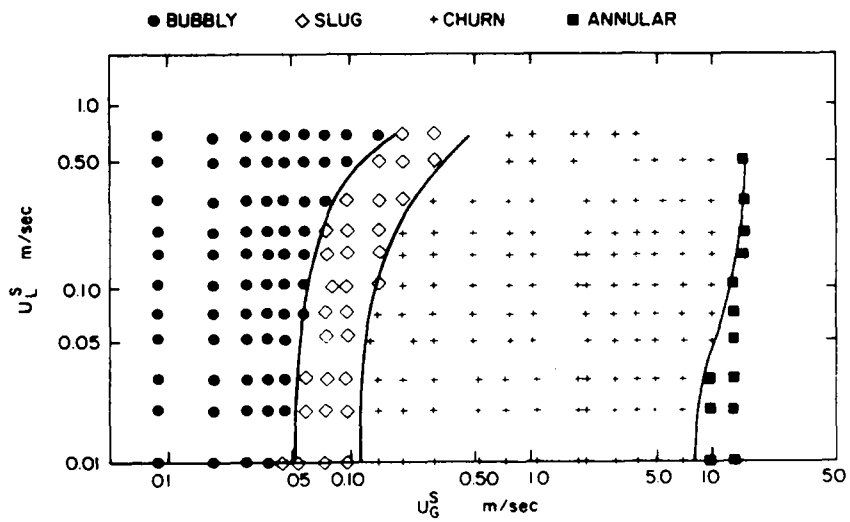

Figure 6. Experimentally observed flow patterns.

and 50 cm/sec liquid velocities) and (c) low density bubbly flow with superficial liquid velocities of 0, 10, 30 and 50 cm/sec). For all measurements the data represent averages of over more than 500 bubbles.

The measured relationship between size and rise velocities of single non-interacting bubbles in stagnant liquid are shown in figure 8. The dotted line represents the rise velocities reported in the literature for an infinite medium and it is clear that the trends are different.

The effect of liquid flow on the bubble velocity has been commonly reported as

$$U = C_L U_L^S + U_0 \quad [1]$$

where U = bubble velocity, C_L = flow correction factor, U_L^S = superficial liquid velocity and U_0 is the rise velocity in stagnant liquid. In the present experimental study C_L was calculated using the measured values of the rise velocity, U and U_0 from figure 8. These are shown in figure 9.

Typical size and velocity distributions for low density bubbly flow in stagnant liquid are shown in figures 10 and 11. In the presence of liquid flow, the rise velocity of bubbles in a low density swarm follow[1] with a value of $C_L = 1.0$ as shown in figure 12.

Cell Taylor Bubbles. These bubbles occupy a large part of the free space in a four rod cell (see figure 5). The tail or skirt of these bubbles frequently break into smaller dispersed bubbles as it rises. Software was developed to discriminate on bubble size and the velocity data associated with these small satellite bubbles was rejected. Results of the experiment show that the average rise velocity of these cell Taylor bubbles is remarkably constant at 24 ± 1 cm/s.

Shroud Taylor bubbles. Shroud Taylor bubbles (10–80 cm^3) were generated in stagnant liquid by the inverted cup technique. As the Taylor bubble rises, liquid falls down the rods and the wall of the shroud. Velocities of these bubbles, measured by the photographic technique described earlier, are shown in figure 13 as curves 3 and 4 representing two sets of data. The spread between these two curves is a measure of the scatter due to the averaging of a relatively small number of bubbles. The constant curve marked 1 is the prediction of Dumitrescu/Taylor theory, while curve 2 shows the prediction of the theory of Grace & Harrison (1967) developed for Taylor bubbles which are penetrated by a single rod.

THEORETICAL MODELS FOR FLOW PATTERN TRANSITIONS

In this section models are developed for each of the transitions using an approach similar to that of Taitel & Barnea (1980) for flow in empty vertical tubes. These models are based on speculation as to the physical mechanism underlying the transition.

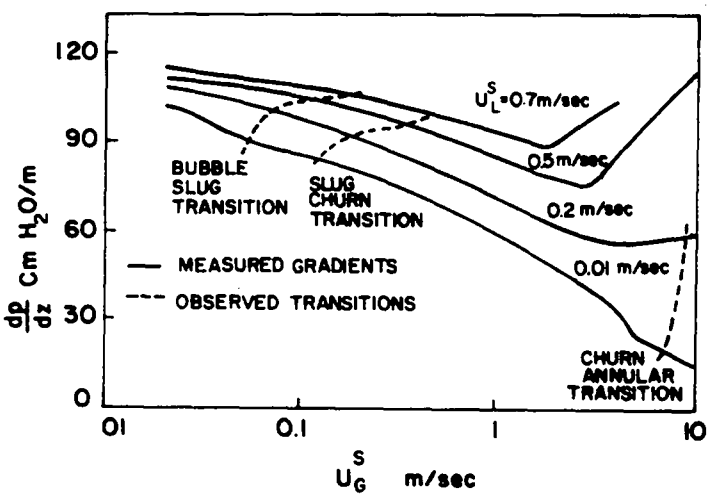

Figure 7. Pressure gradients and flow pattern transitions.

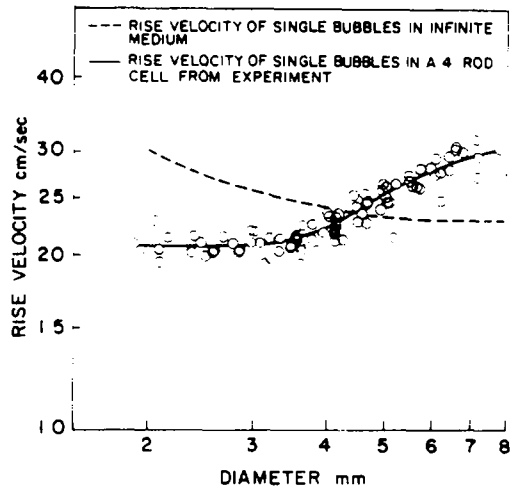

Figure 8. Rise velocity of single bubbles in a 4 rod cell: stationary liquid.

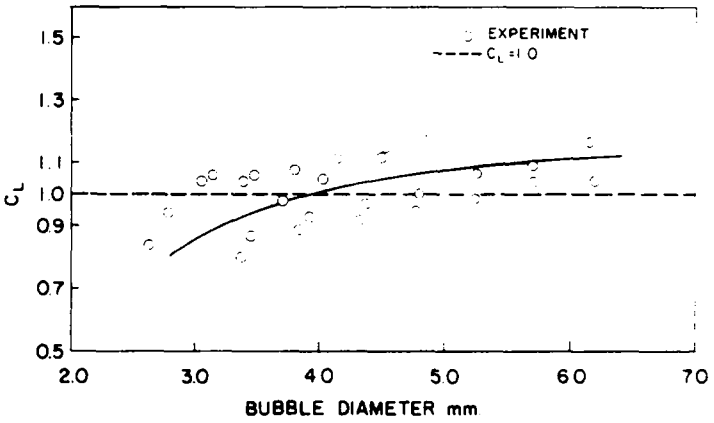

Figure 9. Correction factor C_L for a bubble in a moving liquid.

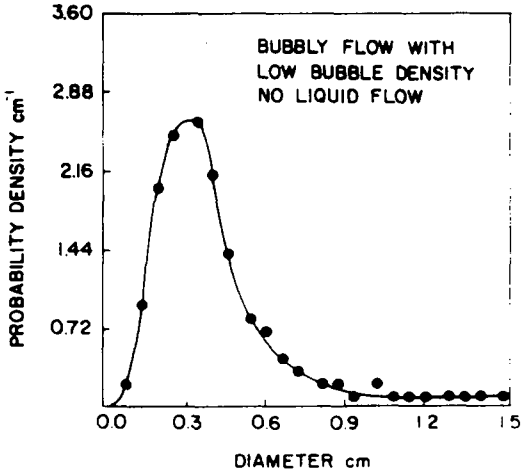

Figure 10. Typical probability density distribution for bubble size.

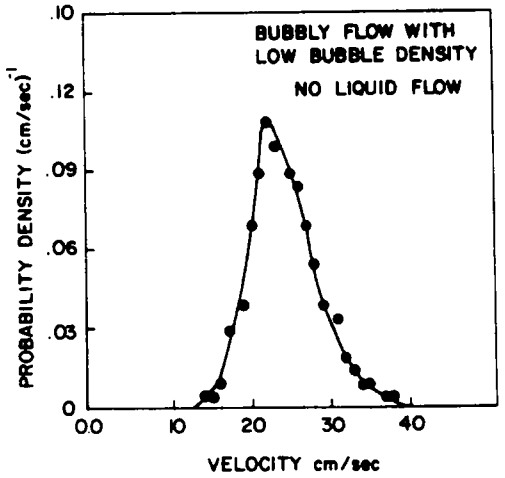

Figure 11. Typical probability density distribution for bubble rise velocity.

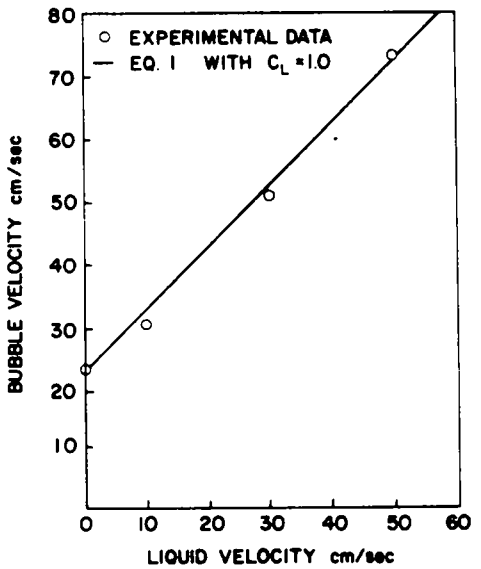

Figure 12. Average bubble velocity for flow with low bubble density.

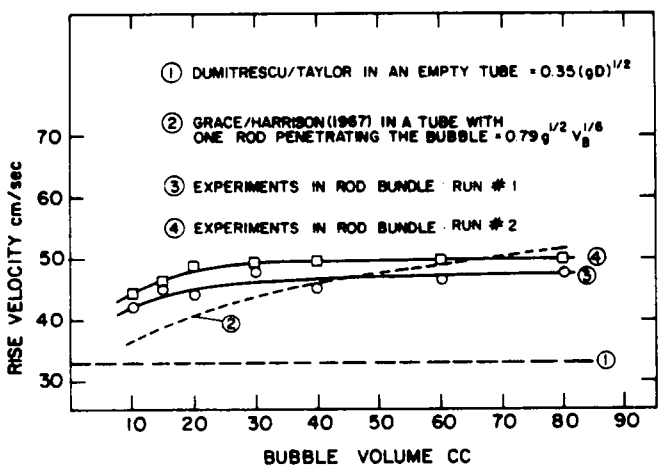

Figure 13. Rise velocity of shroud Taylor bubbles compared with other cases.

(i) *Bubble to slug flow*: When gas is introduced at low flow rates, the gas phase is distributed into discrete bubbles. These bubbles move upward in a zig-zag path with considerable randomness, occasionally colliding, coalescing and forming large bubbles. As the gas rate is increased the bubble size remains about the same, but the bubble density increases and a point is reached where the dispersed bubbles become closely packed so that many collisions occur and the rate of agglomeration increases sharply. This results in a transition to slug flow. If we consider the bubbles to have spherical shape and arranged in a cubic lattice, the void fraction of the gas can be, at most, 0.52. However, as a result of their deformation and random path the rate of collision and coalescence increases sharply at void fractions well below this lattice spacing at which they touch. Therefore, the closest distance between the bubbles before transition must be the one which permits some freedom of motion for each individual bubble. If the spacing between bubbles at which coalescence begins to increase sharply is assumed to be approximately half their radius, this corresponds to a void fraction of 0.25. Thus, $\alpha = 0.25$ is the transition void fraction when all the bubbles are uniformly distributed in the cross-section.

Observation of the bubbles in a rod bundle shows that few bubbles move in the space between any two rods but migrate to the open area which exists between an array of 4 rods. Thus, in the sketch in figure 14, dispersed bubbles are seldom observed in the free space along the line *A–B* but instead are concentrated in the space designated by the circle *C*. Bubbles which originate in the narrow gap migrate to the open region as a result of the Bernoulli force that exists due to the velocity gradient in the cell. Therefore, it is suggested that transition to slug flow takes place when the void fraction in the circle *C* reaches 0.25. This local void fraction α_l can be related to the overall void fraction in all of the free area as

$$\alpha = \frac{[(\sqrt{\{2\}}(p/d) - 1)]^2}{4/\pi(p/d)^2 - 1}\,\alpha_l \qquad [2]$$

where p is the pitch and d is the rod diameter.

In bubbly flow liquid, gas and bubble velocities are related by

$$U_G = U_L + U_0. \qquad [3]$$

Expressing U_G and U_L in terms of superficial flow rates

$$\frac{U_G^S}{\alpha} = \frac{U_L^S}{(1-\alpha)} + U_0 \qquad [4]$$

$$U_G^S = \left[\frac{\alpha}{1-\alpha}\right] U_L^S + \alpha U_0. \qquad [5]$$

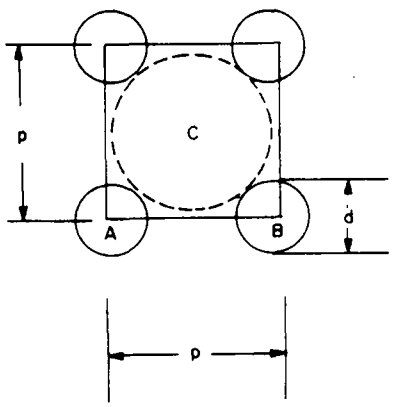

Figure 14. A four rod cell.

For the configuration studied ($p/d = 1.38$) and $\alpha_l = 0.25$ the value of α calculated from [2] is 0.16. Chosing a constant value of $U_0 = 24$ cm/sec it is possible to calculate the transition boundary and this is shown in figure 15 as the dotted line *A*. The solid line marked *A* shows the experimentally observed bubble-slug transition as taken from figure 6.

(ii) ***Slug or bubbly to dispersed bubble pattern.*** At high liquid flow rates, forces due to turbulence cause the gas phase in either slug or bubbly flow to break into small bubbles which are dispersed in the continuous liquid phase. In contrast with the larger bubbles which exist at lower liquid velocities, these bubbles do not display lateral oscillations, collisions or coalescence. Instead they rise linearly and thus remain dispersed. Furthermore, the rise velocity is small compared to the local fluid velocity. This pattern is observed in tubes and has been modelled by Taitel *et al.* (1980). They relate the maximum stable bubble size to the flow conditions and fluid properties through a Weber number criterion. This expression is equated to the relationship which gives the bubble size at which oscillations no longer take place. With these concepts they showed that the equation for the transition is

$$U_L^S + U_G^S = 4.0\left\{\frac{D^{0.429}\left(\frac{\sigma}{\rho_L}\right)^{0.089}}{\nu_L^{0.072}}\left[\frac{g(\rho_L - \rho_G)}{\rho_L}\right]^{0.446}\right\}. \qquad [6]$$

The same condition can be assumed to exist for rod bundles with D taken as the hydraulic diameter of the 4 rod cell. Equation [6] is shown as dotted curve *B–B* in figure 15 for the experimental system and flow properties used in these experiments. Bubbly flow can no longer exist at gas rates so high that the bubbles are packed close enough to be in contact. This will happen when $\alpha = 0.52$ (square lattice). Thus dispersed bubbly flow, the region above *B–B*, must terminate at the right at the condition where $\alpha = 0.52$. From [5] with $U_0 = 0$, the relationship between and the superficial velocities are

$$\alpha = \frac{U_G^S}{U_G^S + U_L^S}.$$

Setting $\alpha = 0.52$ this relationship maps as curve *C–C* in figure 15. Thus, the region to the left of *C–C* and above *B–B* is the predicted zone for dispersed bubble flow. It can be seen from figure

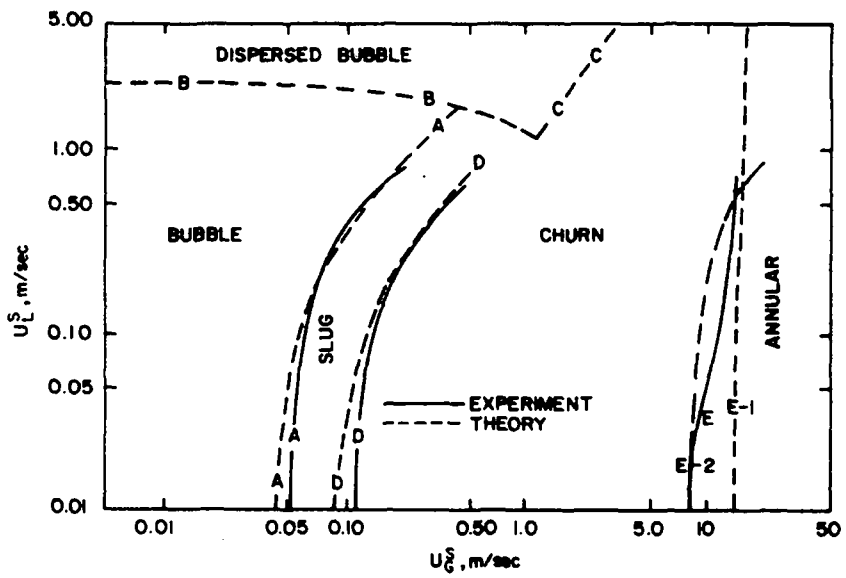

Figure 15. Comparison of theoretical and exprimental transitions.

6 that experiments could not be carried out to high enough liquid rates (due to limitations in pumping capacity) to test this part of the theory in the rod bundle system.

(iii) *Slug to churn flow.* As the gas rate is increased from slug flow, a transition to churn flow pattern takes place. In empty vertical tubes where the Taylor bubbles occupy almost the entire cross sectional area of the pipe, this transition is attributed to entry region behavior (Taitel *et al.* 1980) where slow moving Taylor bubbles are overtaken by faster ones. However, for a rod bundle the transition takes place from "cell type" slug flow to churn flow and the mechanism is quite different due to the absence of the confining walls around each Taylor bubble.

As the gas rate is increased during slug flow, both the number and size of cell Taylor bubbles of the type shown in figure 5 increase. Their size increases to that instead of occupying the center region of a cell (as shown in the cell at the lower left of figure 5b), they grow to cover almost all of the free space in the cell (see the bubble shown at the upper right of figure 5b). At the same time the number of cells occupied by Taylor bubbles increases and eventually the concentration of occupied cells is great enough to cause coalescence. When this happens the liquid being supported by the bubbles suddenly falls downward in a lump, is mixed with the liquid below and starts its ascent again. This behavior of random falling of lumps of liquid is the definition of the churn flow pattern. Thus, in a rod bundle the transition to churn flow is a coalescence phenomena, and therefore this can be expected to take place at the lowest void fraction at which the Taylor bubble density results in contact between bubbles in adjacent cells. If one examines the location of bubble pairs possible in the rod bundle considering an array of cells in the horizontal plane and a series of bubbles in the vertical direction, the minimum voids at which contact can be made is given by the configuration shown in figure 16. The average voids corresponding to this configuration is given by

$$\alpha_T = \frac{\pi(p+d)}{6\cos\theta(2p+d)} \qquad [7]$$

when

$$\theta = \arcsin\frac{p-d}{p+d}.$$

In these experiments with $p = 1.75$ cm and $d = 1.27$ cm α_T at which transition to churn flow should first be observed is 0.335. Now it is possible to use equation [5] with U_0 being the rise velocity of the cell type Taylor bubbles to calculate the relationship between U_{GS} and U_{LS} for this transition. The result appears in figure 15 as a dotted curve marked D is shown to be in reasonable agreement with this experimentally observed transition shown as solid curve D. U_0 in equation [5] was designated as 0.24 m/s, the measured value for cell type Taylor bubbles.

(iv) *Churn to annular transition.* At high gas rates th flow pattern in the rod bundle becomes one of annular film flow. The liquid flows upward along all rod surfaces as thin annular films with gas flowing in the rest of the free area. The liquid interface is highly wavy and the gas carries entrained liquid drops torn from the liquid. For flow in a pipe, Taitel *et al.* (1980) suggested that the mechanism for transition was related to the minimum gas velocity necessary to transport the largest drop in the upward direction. At gas velocities less than this value liquid begins to fall back, accumulate and bridge the pipe only to be thrust upward again, and thus the alternating motion characteristic of churn flow is observed. This mechanism applies when the minimum velocity necessary to lift the film is less than the velocity required to lift the largest drop. This can be expected to be valid for large film thicknesses where it has been observed that the largest drops can be of the order of 5 mm.

This minimum gas velocity was determined from the balance between gravity and drag forces acting on the largest stable drop. The drop size is calculated using a critical Weber

number criteria while the drag coefficient is known to be constant for these large drops. Neglecting the thickness of the liquid film, the result of this analysis is that the churn to annular transition takes place at a superficial velocity which depends only on the fluid properties:

$$U_G^S = 3.1\left[\frac{\sigma g(\rho_L - \rho_G)}{\rho_G^2}\right]^{1/4}. \qquad [8]$$

For the air–water system used in these experiments the equation is plotted as line E-1 in figure 15 and is shown to be in excellent agreement with the data at higher liquid flow rates.

At low liquid rates where the film is very thin the mechanism can be expected to change. Then the liquid film becomes very thin and waves which are the source of the drops are suppressed. Thus, liquid entrainment can no longer be controlling. At this condition of low liquid rate another mechanism comes into play. Fernandes (1981) has shown from experiment that across the churn flow region the simple holdup model for voids in slug flow continues to be valid.

$$\alpha_{ch} = \frac{U_G^S}{U_G}. \qquad [9]$$

As the gas rate is increased the pattern changes to annular and the void is given by

$$\alpha_a = \frac{p^2 - \pi/4(d+2\delta)^2}{p^2 - \pi/4\, d^2} \qquad [10]$$

when p is the pitch, d is the tube diameter and δ is the film thickness.

We speculate that as the gas rate is increased, the condition at which α_{ch} first equals α_a is the condition at which transition takes place. An equation for α_a is developed as follows. Consider a 4 rod cell as defined by the square in figure 14 which has each side of length equal to the ptich, p. A force balance on the gas contained in the cell is:

$$\frac{dp}{dz} + \rho_G s + \frac{P_G}{A_G}\tau_i = 0 \qquad [11]$$

where dp/dz is the pressure gradient in te flow direction, τ_i is the shear acting at the gas liquid interface, P_G is the wetted perimeter of the film and A_G is the flow area for the gas. The following relationships are obtained from geometrical considerations alone.

$$P_G = \pi(d+2\delta) \qquad [12a]$$

$$A_G = p^2 - \frac{\pi(d+2\delta)^2}{4} \qquad [12b]$$

$$\alpha_a = \frac{p^2 - \pi/4(d+2\delta)^2}{p2 - \pi/4\, d^2} \qquad [12c]$$

$$\frac{\delta}{d} = \frac{[1+4C(1-\alpha_a)]^{1/2} - 1}{2} = g(\alpha_a) \qquad [12d]$$

where

$$C = \frac{1}{\pi}\left[\left(\frac{P}{d}\right)^2 - \frac{\pi}{4}\right].$$

As a first approximation the interfacial shear is estimated through a friction factor expression suggested by Wallis (1969)

$$\tau_i = \frac{1}{2} f_i \rho_G U_G^2 = \frac{1}{2\alpha_a^2} f_i \rho_G U_G^2 \quad [13]$$

$$f_i = 0.005 \left(1 + 300 \frac{\delta}{d}\right). \quad [14]$$

Thus, [11] becomes

$$\frac{dp}{dz} + \rho_G g + \frac{0.0025}{C\alpha_a^3 d}[1 + 2g(\alpha_a)][1 + 300\, g(\alpha_a)]\rho_G U_G^{S2}. \quad [15]$$

An overall force balance can be written on both the gas and liquid flowing in the 4 rod cell.

$$\frac{dp}{dz} + [\alpha_a \rho_G + (1 - \alpha_a)\rho_L]g + \frac{P_L}{(A_L + A_G)} \tau_w = 0. \quad [16]$$

Here

$$P_L = \pi d$$

$$A_L + A_G = p^2 - \frac{\pi}{4} d^2$$

$$\tau_w = \frac{1}{2} f_w \rho_L U_L^2 = \frac{1}{2(1 - \alpha_a)^2} f_w \rho_L U_L^{S2}$$

and f_w is estimated according to the suggestion by Wallis (1969), $f_w = 0.005$. Equation [16] then becomes

$$\frac{dp}{dz} + [\alpha_a \rho_G + (1 - \alpha_a)\rho_L]g + \frac{0.0025}{Cd(1 - \alpha_a)^2} \rho_L U_L^{S2} = 0 \quad [17]$$

Equating the pressure drops from [15] and [17] gives an equation relating α_a, U_L^S and U_G^S, once the physical properties ρ_G and ρ_L, the tube diameter, d and pitch, p are specified.

$$(1 - \alpha_a)(\rho_L - \rho_G)g + \frac{0.0025}{Cd(1 - \alpha_a)^2} \rho_L U_L^{S2} =$$

$$= \frac{0.0025}{C d \alpha_a^3}[1 + 2g(\alpha_a)][1 + 300\, g(\alpha_a)]\rho_G U_G^{S2}. \quad [18]$$

Now we search for the intersection of this equation and that given by [9] for the holdup in churn flow. The data on large bubble flow discussed earlier suggest that the rise velocity of these cell type Taylor bubbles can be expressed by

$$U_G = 1.15\,(U_L^S + U_G^S) + U_0 \quad [19]$$

where U_0 is constant at approximately 0.24 m/s as discussed earlier and the coefficient 1.15 can be approximated from figure 9. Equation [9] then becomes

$$\alpha_{ch} = \frac{U_G^S}{1.15(U_G^S + U_L^S) + 0.24}. \quad [20]$$

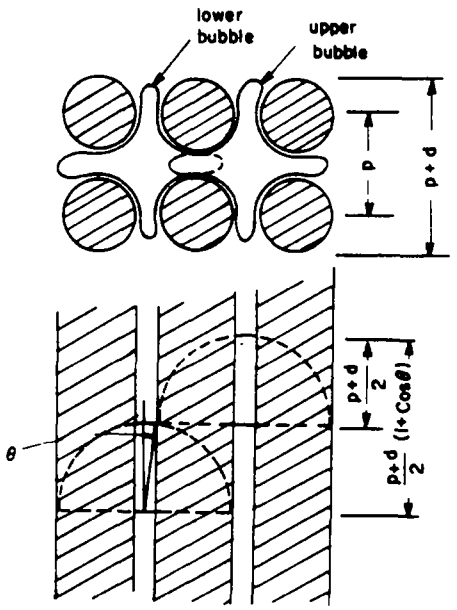

Figure 16. Configuration of cell type Taylor bubbles for lowest voids at transition to churn flow pattern.

This is an equation relating α_{ch}, U_L^S and U_G^S. To find the condition at transition we find the intersection of the two equations where $\alpha_{ch} = \alpha_a$ and this defines the locus of the U_{GS}, U_{LS} pairs at which transition takes place. Setting p, d and the fluid properties to meet the conditions of these experiments results in the prediction shown by the dotted curve E-2 in figure 15. It is seen that the experimental data (solid curve E) is bracketed by the two models. As expected the agreement is best at high liquid rates with the entrainment model and at low rates with the void fraction matching model.

As an independent test of the validity of the film model, measurements were made of pressure gradient and flow patterns across the transition from churn to annular flow using transducers located in the pressure taps shown in figure 2. The results are shown as the data symbols in figure 17 using dimensionless coordinates

$$\Delta P^* = -\frac{1}{(\rho_L - \rho_G)g}\frac{dp}{dz}$$

$$U_G{}^{S*} = \left[\frac{\rho_L}{gd(\rho_L - \rho_G)}\right]^{1/2} U_G{}^S.$$

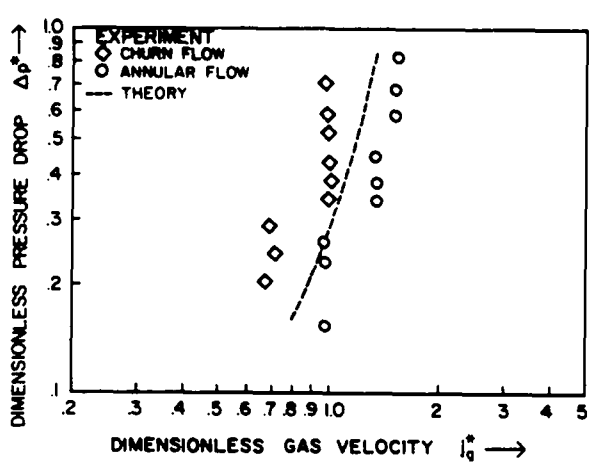

Figure 17. Dimensionless pressure drop at the churn–annular transition.

The dotted curve is the prediction of either [15] or [17] along the locus of U_{LS}, U_{GS} pairs where $\alpha_{ch} = \alpha_a$. Agreement is seen to be satisfactory.

The transitions predicted by these models have been compared with the data of Williams & Peterson (1978) and of Bergles *et al.* (1968). In both cases the system was a boiling steam-water system. Williams & Peterson report data at three pressure levels (2.8×10^6, 8.3×10^6 and 13.8×10^6 N/m^2) in a rod linear array, while Bergles *et al.* operated at a pressure of 6.9×10^6 N/m^2 with a 4 rod square array. Figures 18–20 compare the Williams & Peterson data with the prediction of the models presented in this work. The solid curves display the location and the range of the data in superficial velocity space, while the dotted curves represent the transition curves as calculated from the models using the fluid properties and geometry of the system. Transition E-2 for this configuration was calculated assuming that a film existed on the shroud of equal thickness and interfacial shear as on the rods.

At the lowest pressure (figure 18) Williams and Peterson report only bubbles, slug and annular flow since churn flow is not included in their lassification scheme. Slug flow is described as that pattern where the diameter of the bubbles becomes approximately equivalent to a subchannel of equivalent diameter, while annular flow is that condition where a continuous axial filament of vapor exists. Thus, they do not discriminate between the churn and slug patterns. Figure 18 shows reasonably satisfactory agreement for the two transitions observed. At the higher pressure conditions (figures 19 and 20) no slug flow was observed. This is exactly what would be predicted by the model. The aurhors define froth flow as a condition of highly packed bubbles in the absence of coalescence to larger bubbles characteristic of slug flow. We consider this simply part of the dispersed bubble pattern and mark no distinction. At 8.3×10^6 N/m^2 (figure 19) the annular transition is equally well predicted by the drop lift (E-1) or the matching voids (E-2) model. At the highest pressure (figure 20) the drop lift model seems more satisfactory.

A comparison with the data of Bergles *et al.* (1968) appears in figure 21. The transition from bubbly to slug flow is predicted reasonably well. For the transition to annular flow at low liquid rates the voids matching model appears to give reasonable agreement while at higher rates the drop mechanism is better. For both the experiments of Williams & Peterson as well as Bergles *et al.* the agreement seems especially encouraging when one considers that (a) with only 4 rods the effect of

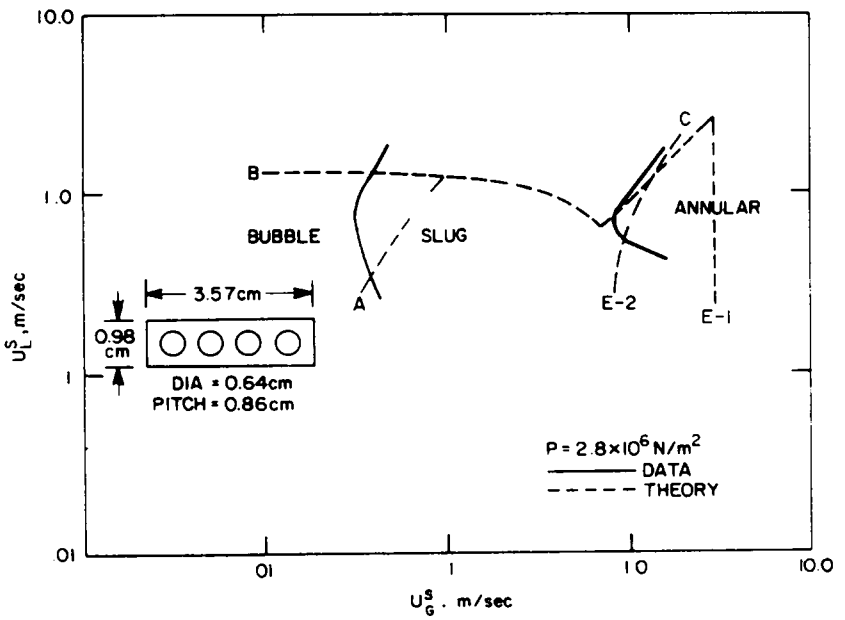

Figure 18. Comparison of theory with Williams and Peterson data for steam-water at 2.8×10^6 N/m^2.

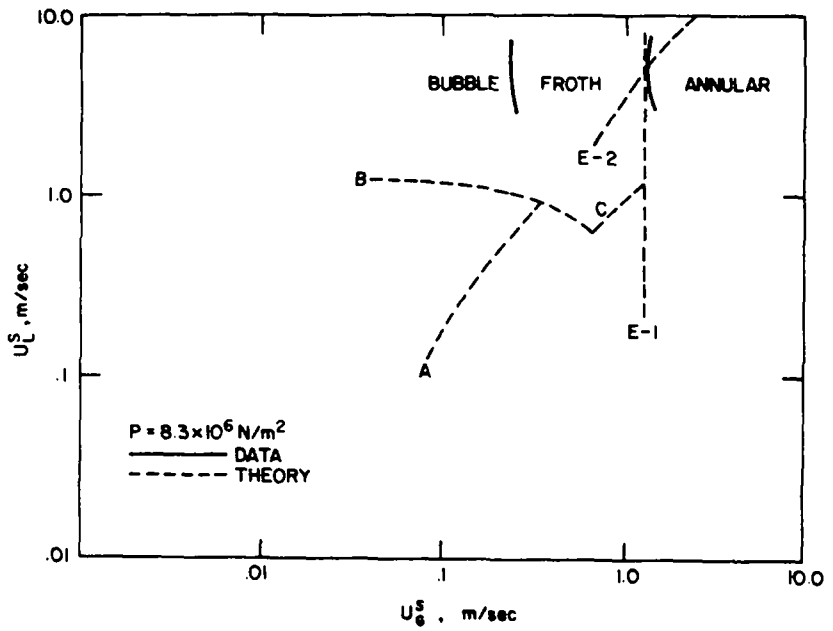

Figure 19. Comparison of theory with Williams and Peterson Data for steam–water at 8.3×10^6 N/m^2.

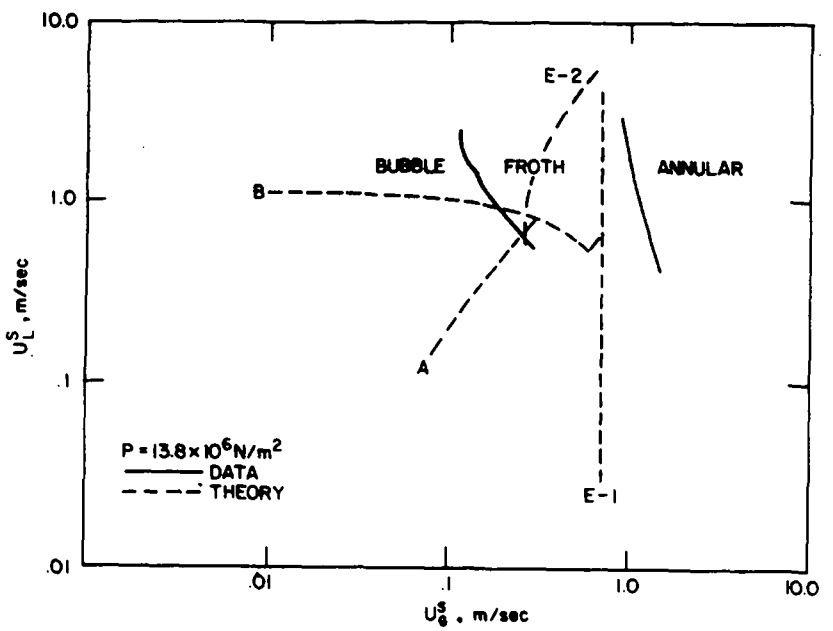

Figure 20. Comparison of theory with Williams and Peterson data for steam–water at 13.8×10^6 N/m^2.

the shroud can be very important, (b) the models are not designed to accommodate the boiling process which took place in the Williams and Peterson experiments and (c) the observations were admittedly very difficult to make.

CONCLUSIONS AND RECOMMENDATIONS

Models developed here for flow pattern transition in a vertical rod bundle show reasonable agreement with new data presented for air–water in a 24 rod matrix, as well as with steam–water data in 4 rod array experiments of others. The correlations and models proposed must still be tested with data for other rod spacing and size and for other fluid pairs before they can be used with confidence in a general way.

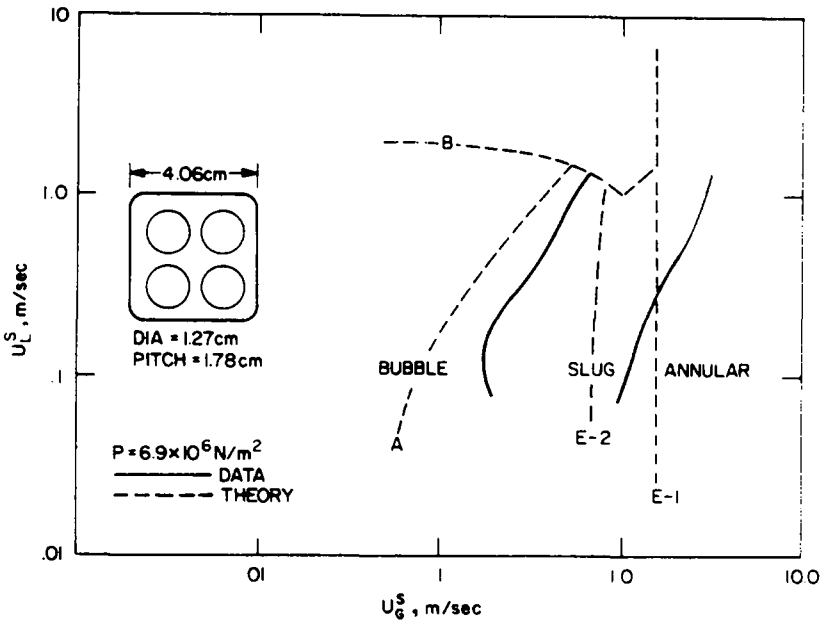

Figure 21. Comparison of theory with Bergles *et al.* data for steam–water at 6.9×10^6 N/m^2.

Acknowledgement—This work was supported by the U.S. Nuclear Regulatory Commission.

REFERENCES

BERGLES, A. E., ROOS, J. P. & BOURNE, J. G. 1968 *Investigation of boiling flow regimes and critical heat flux*, NYO-3304–13. Dynatech Corporation, Cambridge, Massachusetts.

DAVIES, R. M. & TAYLOR, G. 1950 The mechanics of large bubbles rising through extended liquids and through liquids in tubes. *Proc. Roy. Soc.* **200A**, 375–390.

DUMITRESCU, D. T. 1943 Strömung an Einer Luftblase im Senkrechten Rohr. *ZAMM*, **23**, 139–149.

FERNANDES, R. 1981 Experimental and theoretical studies of isothermal upward gas–liquid flow in vertical tubes, Ph.D. Thesis, University of Houston.

GRACE, J. R. & HARRISON, D. 1967 Influence of bubble shape on the rising velocities of large bubbles. *Chem. Engng Sci.* **22**, 1337–1347.

HINZE, J. O., 1955, Fundamentals of the hydrodynamic mechanism of splitting in dispersed processes. *A.I.Ch.E.J.* **1**, 289–295.

SEMIAT, R. & DUKLER, A. E. 1981 The simultaneous measurement of size and velocity of bubbles or drops. *A.I.Ch.E.J.* **27**, 148–159.

TAITEL, Y. & BARNEA, D. 1980 Modelling flow pattern transitions for steady, upward gas-liquid flow in vertical tubes. *A.I.Ch.E.J.* **26**, 345–354.

VENKATESWARARAO, P. 1981 Studies related to flow pattern transitions for two-phase flow in a vertical rod bundle array, M. S. Thesis, University of Houston.

WALLIS G. B. 1969 *One-Dimensional Two Phase Flow*. McGraw Hill, New York.

WILLIAMS, C. L. & PETERSON, JR., A. C. 1978 Two phase flow patterns with high-pressure water in a heated four-rod bundle. *Nuc. Sci. & Engng* **68**, 155–169.